

# Seasonal variability of the mixed layer in the central Bay of Bengal and associated changes in nutrients and chlorophyll

Jayu Narvekar and S. Prasanna Kumar

Physical Oceanography Division, National Institute of Oceanography, Dona Paula, Goa-403 004, India.

---

## Abstract

Hydrographic data from NODC and RNODC were used to study the seasonal variability of the mixed layer in the central Bay of Bengal ( $8^{\circ}\text{N}$  to  $20^{\circ}\text{N}$  and  $87^{\circ}\text{E}$  to  $91^{\circ}\text{E}$ ), while meteorological data from COADS were used to explore atmospheric forcing responsible for the variability. The observed changes in the mixed-layer depth clearly demarcated a distinct north-south regime with  $15^{\circ}\text{N}$  as the limiting latitude. North of this latitude mixed-layer depth remained shallow ( $\sim 20$  m) for most of the year without showing any appreciable seasonality. Lack of seasonality suggests that the low-salinity water, which is perennially present in the northern Bay, controls the stability and mixed-layer depth. The observed winter freshening is driven by the winter rainfall and associated river discharge, which is advected offshore under the prevailing circulation. The resulting stratification was so strong that even a  $4^{\circ}\text{C}$  cooling in SST during winter was unable to initiate convective mixing. In contrast, the southern region showed a strong semi-annual variability with deep MLD during summer and winter and a shallow MLD during spring and fall intermonsoons. The shallow MLD in spring and fall results from primary and secondary heating associated with increased incoming solar radiation and lighter winds during this period. The deep mixed layer during summer results from two processes: the increased wind forcing and the intrusion of high-salinity waters of Arabian Sea origin. The high winds associated with summer monsoon initiate greater wind-driven mixing, while the intrusion of high-salinity waters erodes the halocline and weakens the upper-layer stratification of the water column and aids in vertical mixing. The deep MLD in the south during winter was driven by wind-mixing when the upper water column was comparatively less stable. The deep MLD between  $15^{\circ}$  and  $17^{\circ}\text{N}$  during March to May cannot be explained in the context of local atmospheric forcing. We show that this is associated with the propagation of Rossby waves from the eastern Bay. We also show that the nitrate and chlorophyll distribution in the upper ocean during spring intermonsoon is strongly coupled to the mixed-layer depth,

whereas during summer river runoff and cold-core eddies appear to play a major role in regulating the nutrients and chlorophyll.

## **1. Introduction**

The Bay of Bengal, situated in the eastern part of the northern Indian Ocean, is a tropical basin, which is landlocked in the north and is forced by a semi-annually reversing wind system, the monsoon. During winter (northeast) monsoon (November-February), the winds are weak ( $\sim 5$  m/s) and from the northeast. These northeast trade winds bring cool and dry continental air to the Bay of Bengal. In contrast, during the summer (southwest) monsoon (June-September) the strong ( $\sim 10$  m/s) southwest winds bring humid maritime air into the Bay of Bengal. The unique feature of the Bay of Bengal is the large seasonal freshwater pulse, which makes the waters of the upper layers less saline and highly stratified (Fig.1). This seasonal freshening is brought about by the excess precipitation over evaporation ( $\sim 2$  m  $\text{yr}^{-1}$ , Prasad, 1997) and also by the freshwater influx from the adjoining rivers ( $1.625 \times 10^{12}$  m<sup>3</sup>  $\text{yr}^{-1}$ , Subramanian, 1993).

The surface circulation within the basin, however, reverses semi-annually; it is not strictly in accordance with the wind reversal but appears to lead it. During the end of winter, in February, when the winds are still northeasterly, the current along the western boundary reverses and flows northward. This northward flowing East India Coastal current (EICC) peaks during March-April (spring intermonsoon), when the winds are weak but possess anticyclonic curl (Shetye et al., 1993). Open-ocean circulation during this period is the best organized with an anticyclonic, subtropical gyre, and EICC forms the western limb of this circulation. In May, prior to the intensification of summer (southwest) monsoon, the spring-time anticyclonic

circulation collapses and the EICC weakens. In July, when the southwest monsoon is at its full strength, the EICC weakens further and even reverses to a southward flow in the northern part (Shetye et al., 1991). The open-ocean circulation at this time of the year consists of multiple gyres, recirculations, meanders and eddies. In September, when the southwest monsoon weakens, the EICC reverses, flowing towards the south almost along the entire coast, forming a part of the cyclonic gyre. The southward EICC peaks in December and decays in January, completing its annual cycle.

Apart from the above-mentioned large seasonal freshening and semi-annual reversal of the upper-layer circulation, the Bay of Bengal also is a site of severe tropical cyclones. The cyclones are generated during the spring (April-May) and fall (October) intermonsoons, and are associated with large-scale flooding and destruction in the coastal regions.

In the past, several studies attempted to understand the complex nature of the circulation and hydrography in the Bay of Bengal (see Varkey et al., 1996; Schott and McCreary, 2001; Shankar et al., 2002). An increasing number of recent studies suggest the role of remote forcing in aiding the semi-annual variability of the upper-layer circulation in the Bay (Potemra et al., 1991; Yu et al., 1991; Perigaud and Delecluse, 1992; Prasanna Kumar and Unnikrishnan, 1995; McCreary et al., 1993 & 1996, Shetye et al., 1996; Vinayachandran et al., 1996; Shankar et al., 1996; Eigenheer and Quadfasel, 2000). The remote forcing could arise by a variety of mechanisms, such as planetary waves originating at the eastern boundary excited by the energy radiated by the coastal Kelvin wave, planetary waves generated by the variability in the local alongshore winds, and the interior Ekman pumping during the peak of summer and winter monsoons. It is natural to expect that

these semiannual atmospheric forcings as well as the remote forcing would modulate the thickness of the upper ocean by altering the thermal and mechanical inertia of the layer. In the past there were a few studies to understand the changes in the mixed layer in the Indian ocean, including the Bay of Bengal, based on either individual cruises (e.g., Molinari et al., 1986; Rao, 1986; Sanilkumar et al., 1997; Gopalakrishna et al., 1988) or climatology (e.g., Rao et al., 1989; Monterey and Levitus, 1997). More recently, Shenoi et al. (2002) and Prasad (2004) used climatological data of Levitus et al. (1994) and Conkright et al. (1998), respectively, to compare the mixed-layer variability in the Arabian Sea and the Bay of Bengal. The former study discusses various processes that are responsible for the mixed-layer heat budget for both the seas, while the latter used a one-dimensional model to address the mixed-layer variability. However, none of the earlier studies addressed the role of advection or remote forcing in regulating the mixed layer. In the present study we used more extensive and recent data from Indian research vessels as well as Argo floats to analyze the seasonal variability of the mixed layer and explored the atmospheric forcing in mediating such changes, including the remote forcing and advection of high salinity waters from the Arabian Sea. We also explored the associated chemical and biological changes in the water column. We chose the central Bay of Bengal to eliminate the direct effect of boundary processes, such as river discharge and associated plumes, boundary currents, coastal upwelling, etc. and to capture the open-ocean variability in describing the processes responsible for such changes.

## **2. Data and method**

The Bay of Bengal, in general, is a data-poor region compared to the rest of the Indian Ocean. For the present study we have relied upon two types of data: hydrographic data to describe the mixed layer variability and atmospheric data to understand the processes that bring about the changes in the upper layers.

### ***2.1. Hydrographic data***

The hydrographic data used for the study were extracted mainly from the National Oceanographic Data Center (NODC) CD-ROM, which contains temperature and salinity data from hydrocast as well as conductivity-temperature-depth (CTD) casts for the period 1900-1992 (Levitus et al., 1994). In addition, data were also used from the Responsible National Oceanographic Data Centre (RNODC) at Goa, which contains hydrocast and CTD data, for the period 1976-1997, collected by Indian research vessels. Apart from this we have also utilized CTD data collected under the programme Bay of Bengal Process study (BOBPS) during 2001-2003 and Argo data during the period 2001-2004. From preliminary examination of the data distribution it was found that the domain between 87 and 91°E has reasonably good spatio-temporal coverage. Hence the region covering 4-20°N and 87-91°E was selected for the present study (Fig.1). The following quality control procedures were applied to obtain quality-controlled data for analysis.

At first, duplicate profiles as well as those with obvious errors were excluded by visual inspection. Then, profiles with depth less than 50m were eliminated. In all a total of 492 profiles of temperature and salinity were available after the quality control, out of which 169 profiles were obtained from hydrocast, 187 profiles from CTD and 136 profiles from Argo data.

From the data distribution, it was evident that to obtain a monthly mean coverage it was necessary to prepare spatial mean profiles on  $2^{\circ}$  latitude by  $4^{\circ}$  longitude grids. Table 1 gives the number of profiles on each of the  $2^{\circ} \times 4^{\circ}$  grids. Based on these profiles monthly mean climatology of temperature and salinity were prepared on  $2^{\circ} \times 4^{\circ}$  grids to a depth of 500m. Monthly mean temperature and salinity data were used to calculate the sigma-t values (UNESCO, 1981). Since we see a large temporal gap in the data south of  $8^{\circ}\text{N}$  (Table 1), we restrict our analysis to data north of  $8^{\circ}\text{N}$ .

## ***2.2 Atmospheric data***

Atmospheric data used in the study were derived from Comprehensive Ocean Atmosphere Data Set (COADS) (Da Silva et al., 1994), which contains the monthly mean climatology of the surface meteorological observations, such as incoming short-wave radiation, zonal and meridional wind, and evaporation minus precipitation (E-P) on a  $2^{\circ} \times 2^{\circ}$  grid for the period 1945-1989. The net heat flux was derived from the NOC 1.1 (formerly SOC) Air-Sea Flux Climatology (Josey et al., 1998).

## ***2.3 Nitrate and chlorophyll data***

The nitrate and chlorophyll data were obtained from the RNODC during the period 1951-1997. For the present study we used data from the upper 100 m of the water column for the same grid locations as those of hydrographic data. The data were physically scanned to identify and eliminate obvious errors and duplicate profiles. In all, 89 nitrate profiles and 83 chlorophyll profiles were available after the quality control. The paucity of data forced us to construct seasonal mean profiles instead of monthly

means (Table 2). It is evident from the data distribution that even on a seasonal scale the number of profiles in each of the grid units is scanty. Further, only during spring intermonsoon (March-May) and summer (June-September) monsoon profiles of both nitrate and chlorophyll exist in a given grid unit. For example, during spring intermonsoon both nitrate and chlorophyll profiles are available from 8°-20°N, where as in summer they are available only from 12°-20°N. However, the fall (October) intermoonsoon and winter monsoon (November-February) data were not used for the present study because of the lack of simultaneous profiles of nitrate and chlorophyll in most of the grid under consideration.

#### ***2.4 Remote sensing data***

Since the *in-situ* chlorophyll data are limited in both space and time, we used chlorophyll concentrations derived from global 9-km monthly mean SeaWiFS data for the period September 1997 to December 2004 (<http://reason.gsfc.nasa.gov/OPS/Giovanni/ocean.seawifs.shtml>) to compare with surface distributions. We also used merged sea-level anomalies of Topex/Poseidon ERS1/2 series satellites obtained from AVISO live access server (<http://las.aviso.oceanobs.com>) for the period October 1992 to January 2004, which gives 7-day snapshots having a spatial resolution of 1/3<sup>rd</sup> of a degree, to prepare monthly mean climatology of sea-level anomaly and to compute geostrophic velocity.

### **3. Selection of mixed-layer depth**

Two types of mixed layer depth (MLD) definitions have been most commonly used in the literature: one based on specifying a difference in

temperature or density from the surface value (Wyrтки, 1964; Levitus, 1982; Schneider and Muller, 1990) and the other based on specifying a gradient in temperature or density (Bathen, 1972; Lukas and Lindstrom, 1991). It is important to examine the distribution of properties within the upper layer before any such criteria are applied. Since the Bay of Bengal comes under the semi-annual forcing of monsoons, the vertical profiles of temperature, salinity and sigma-t are presented for a 2-degree grid centered at 9°N and 19°N latitude along 89°E for the month of August (summer) and February (winter) (Fig.2).

The vertical profiles indicate that the isothermal, isohaline and isopycnal layers, in general, seem to coincide in the upper ocean irrespective of the season in the southern part of the central Bay of Bengal, but in the northern Bay temperature and salinity have a different vertical structure. Usually, the temperature shows an isothermal layer within which the salinity increases rapidly with depth. This is associated with freshening due to the river runoff as well as precipitation during summer. Hence, the criteria for defining the MLD should take into account the density variation rather than temperature or salinity. In the present study we defined MLD as the depth at which the density (sigma-t) exceeds  $0.2 \text{ kg m}^{-3}$  from its surface value. For this purpose, the monthly mean temperature, salinity and sigma-t profiles were interpolated onto 1 m-depth intervals by the cubic spline method.

#### **4. Results**

The time-latitude distribution of mixed-layer depth showed a clear-cut north-south regime with strong semi-annual variability south of 15°N and lack of distinct seasonality towards the north. In general, south of 15°N,



deeper MLD ( $>30$  m) occurred during June to September and November until February (Fig.3). In the north, north of  $15^{\circ}\text{N}$ , MLD showed a steady decrease with latitude, attaining the lowest value of 10 m. Interestingly, MLD remained shallow throughout the year. An anomaly was the occurrence of a patch of 30 m deep MLD between  $15$  and  $17^{\circ}\text{N}$  during March to June when MLD was shallow in the south.

The sea-surface-temperature (SST) distribution showed a gradual heating from February to June, with its peak value of  $31^{\circ}\text{C}$  in April (Fig.4). From June until October, SST cooled slowly, by about  $1.5^{\circ}\text{C}$ , except between  $14$  and  $17^{\circ}\text{N}$ , where warming was noticed during August-September. Rapid cooling occurred in the north (north of  $13^{\circ}\text{N}$ ) from November until February, attaining the lowest temperature of  $25.5^{\circ}\text{C}$  in January. In the south (south of  $13^{\circ}\text{N}$ ), however, SST was warmer throughout the year. Thus, because of winter cooling, in the north the amplitude of the seasonal signal ( $\sim 5^{\circ}\text{C}$ ) was much higher than that in the south ( $\sim 3^{\circ}\text{C}$ ).

The sea-surface-salinity (SSS) distribution also showed a distinct north-south difference, with higher salinity towards the south (Fig.5). In general, SSS showed a decrease from 34 in the south to 30 in the north. However, in the south (south of  $13^{\circ}\text{N}$ ) the increase was only 1 but with weak seasonality. In the north (north of  $13^{\circ}\text{N}$ ) the salinity showed rapid decrease with latitude, a total of about 3.5, as well as a strong seasonality. A low-salinity plume with salinity 30 appeared in the north during June and steadily moved southward, reaching near  $17^{\circ}\text{N}$  by September. Another low salinity plume (31) was seen in the region between  $15$  and  $17^{\circ}\text{N}$  during January, and was also seen spreading southward until March. The low-salinity plume during June to September in the north must be associated with the freshwater discharge from the Ganges-Brahmaputra river system coupled with the

summer-monsoon precipitation. In the south, the northward extension of the 34 isohaline from August to October appears to be the manifestation of the intrusion of Arabian Sea High Salinity Water (ASHSW). The summer-monsoon current during this time of the year flows from west to east, replacing the north equatorial current (NEC), carrying with it the ASHSW, which intrudes into the Bay and increases the salinity.

Thus, in the south, the shallowest MLD (<20 m) was, in general, associated with the warmest SST and a patch of relatively low salinity. However, the patch of shallow MLD centered at 9°N during June-July could also be the manifestation of a sub-surface cold-core eddy, which is capable of making the mixed layer shallow (see Prasanna Kumar et al., 2004). The occurrence of a deep MLD did not always coincide with the region of high salinity. For example, during October until December, when the salinity between 8 and 13°N remained the same, the MLD showed a gradual increase. Similarly, deep MLDs also did not show a strong relation with SST. For example, a comparatively deep MLD between 15 and 17°N occurred during March to May, when SST showed an increase. In the north, shallow MLDs were associated with low salinity but did not show any relationship with the seasonality in SST. In order to understand the above variability, we analyzed the physical forcing that regulates MLD, such as incoming short-wave radiation, wind and freshwater flux (evaporation-precipitation; E-P).

The incoming short-wave radiation exhibited a biannual cycle in the central Bay of Bengal, with a strong primary and a weak secondary heating (Fig.6). The primary heating in this region was from February to May with a peak in March-April ( $290 \text{ W/m}^2$  north of 10°N), corresponding to spring intermonsoon. The secondary heating was seen predominantly in the south

(south of 15°N) during August-September, corresponding to fall intermonsoon, with a peak value of 225 W/m<sup>2</sup>. The incoming short wave radiation was reduced by about 60 W/m<sup>2</sup> during summer, while the reduction was about 100 W/m<sup>2</sup> in winter from its spring intermonsoon value. The observed seasonal variability in SST appeared consistent with the changes in the incoming short-wave radiation except during the fall intermonsoon, when it did not show a corresponding proportionate increase. Nevertheless, a marginal warming in the north (notice the shaded region inside the 28.5°C contour in Fig.4) was perceptible.

The net heat flux showed heat gain by the ocean during February to November, with a peak of 130 W/m<sup>2</sup> in April and heat loss from the ocean during November to January (Fig.7). The wind speed also showed a semi-annual variability (Fig.8), with high speeds in June (9.5 m/s) and December-January (6.5 m/s). The wind speed decreased from winter to spring intermonsoon (March-April), attaining its annual minimum of 4 m/s. From spring intermonsoon to summer the wind speed showed rapid increase. Once again, from summer to fall intermonsoon the wind speed decreased to less than 6 m/s. It could be seen that, in general, in the south the region of deep MLD (Fig.3) was located where the maximum wind speed occurred. However, in the north the shallow MLD was encountered even when wind speed was high.

The freshwater flux (E-P) north of 13°N was positive during November until April and negative during the rest of the time (Fig. 9). However, evaporation exceeded precipitation during January until April, even in the south. A large pulse of precipitation amounting to 240 mm/month during June-July north of 13°N coincides with the low-salinity region (Fig.5). Another pulse of precipitation of 120-140 mm/month was noticed during

October to December south of 12°N. Incidentally, we do see a corresponding freshening of the surface waters by way of decrease in salinity of 0.5 in this region (Fig.5). It may be recalled that a low salinity plume (~31) was noticed between 15 and 17°N, but there was no corresponding signal in the freshwater flux. In fact E-P showed a net evaporation amounting to 80 mm/month from this region during this period. This calls for another mechanism for the observed freshening such as advection of fresh water from Krishna and Godavari rivers.

In order to explore the effect of mixed-layer variability and stratification on the upper-ocean nutrients and biology, we analyzed nitrate and chlorophyll data in the upper 100 m depth of the water column. During spring intermonsoon (March-May) the upper 30 m of the water column showed very low or undetectable levels of nitrate, with 0.5  $\mu\text{M}$  below 40 m and 1  $\mu\text{M}$  at about 50 m (Fig.10a). A strong nitracline was noticed below 60 m with rapid increase of nitrate with depth. Satellite-derived chlorophyll distribution (Fig.11a) showed low concentrations (0.15  $\text{mg}/\text{m}^3$ ) in the south and an increasing trend towards the north. Though satellite-derived chlorophyll concentration appears to be over-estimated in comparison to *in-situ* measurements, the trend was consistent with the chlorophyll distribution measured *in-situ* (Fig.11b). This gave us confidence to derive inferences from the *in-situ* measurements, though the data were limited. Consistent with nitrate distribution the vertical chlorophyll distribution also showed very low concentrations ( $\sim 0.05\text{-}0.1 \text{ mg}/\text{m}^3$ ) in the upper 30 m (Fig.11b), but the concentrations increased steadily with depth, attaining a maximum of 0.5  $\text{mg}/\text{m}^3$  at about 80 m. Below this deep chlorophyll maximum (DCM), the chlorophyll concentrations once again decreased.

The vertical distribution of nitrate during summer showed prominent oscillations in the nutricline with an up-sloping followed by a down-sloping centered at 14°N and 19°N respectively (Fig.10b). The nitrate level in the upper 20 m in the north (north of 16°N) was about 2  $\mu\text{M}$ . Though the number of nitrate profiles in each of the 2-degree bins (Table 2) during summer were more compared to spring intermonsoon, one needs to exercise caution in drawing inferences. The observed distribution pattern could be either an artifact of less data or a real feature of the Bay during this time of the year. The up/down sloping of nitrate isopleths centered at 14 and 19°N indicates the existence of cold-core eddies. In fact recent measurements in the Bay of Bengal during summer 2001 did show the occurrence of at least two cold-core eddies along 88°E (Prasanna Kumar et al., 2004), which lends support to our inference that this was a real feature. Once again the satellite-derived chlorophyll concentrations (Fig.11c) showed a distribution pattern similar to that of the surface chlorophyll obtained from *in-situ* measurements (Fig.11d). Consistent with nitrate levels chlorophyll distribution showed high concentrations up to 0.5  $\text{mg}/\text{m}^3$  in the upper 20 m layer in the north (Fig.11d). However, in the south (south of 16°N), though the nitrate concentrations were in the range of 0.5-1  $\mu\text{M}$  in the upper 50 m, the chlorophyll concentrations were extremely low ( $\sim 0.05 \text{ mg}/\text{m}^3$ ). In the north (north of 17°N) chlorophyll concentrations were extremely low below 50 m.

## 5. Discussion

The observed changes in the mixed-layer depth clearly demarcated a distinct north-south regime with 15°N as the limiting latitude. North of this latitude mixed-layer depth remained shallow ( $\sim 20 \text{ m}$ ) for most of the year, except

during March to May between  $15^{\circ}$  and  $17^{\circ}\text{N}$ , without showing any appreciable seasonality. In contrast, the southern region showed a strong semi-annual variability with deep MLD during summer and winter. This could be understood in the context of incoming solar radiation, prevailing winds and freshwater flux (E-P). Both incoming solar radiation and wind showed a weak semi-annual variability while E-P exhibited an annual signal. Under normal circumstances an increased wind speed would lead to strong vertical mixing and deep mixed layer, while decreased wind speed would lead to weak vertical mixing and shallow mixed layer. In contrast an increased solar heating would lead to a decrease in MLD due to strong stratification, while a decrease in solar heating would lead to an increase in MLD due to weak stratification. Lack of seasonality in the north suggested that MLD was not influenced by the above two atmospheric forcings. The surface salinity distribution showed that in the north salinity remained less than 33 all through the year (varying from 29.5 to 32.5), while E-P was negative during May to November. The lowest salinity of less than 30 occurred in the north during summer, when E-P was negative and at its peak, while that between  $15^{\circ}$  and  $17^{\circ}\text{N}$  latitude occurred during January, when E-P was positive. This suggested that salinity in the north was controlled by E-P in addition to the freshwater input from the Ganges-Brahmaputra river system. However, the freshening between  $15^{\circ}$  and  $17^{\circ}\text{N}$  during January, when evaporation overwhelmed the precipitation in the Bay, must be driven by the advection of freshwater from the adjoining rivers such as Godavari, Krishna and Pennar along the east coast of India and Irrawady along the west coast of Myanmar (Fig.1). It may be noted that during winter as the northeast trade winds move over the Bay, they pick up moisture, leading to rainfall in the southern coastal region of the east coast of India. To explore

whether winter rainfall and associated river discharge were significant, we extracted rainfall data for coastal Andhra Pradesh (for the period 1871-2000) and Yangon (for the period 1961-1990), from <http://www.monsoondata.org/hist/climsubdiv.html> and <http://www.worldweather.org/180/c00232.htm>, respectively, while the river discharge data for Godavari (1901-1979), Krishna (1901-1979) and Pennar (1965-1979) were obtained from <http://grdc.bafg.de/servlet/is/2781/>. The total winter rainfall during November to February (Fig.12a) for coastal Andhra Pradesh was about 185 mm, which accounted for 18.8% of the annual rainfall, while that for Yangon was 74 mm which was only 2.7% of the annual rainfall. Commensurate with the winter rainfall, the freshwater discharge during December to March from Godavari, Krishna and Pennar were  $4400 \times 10^6 \text{ m}^3$ ,  $2897 \times 10^6 \text{ m}^3$  and  $880 \times 10^6 \text{ m}^3$  respectively (Fig.12b). Though the winter rainfall was less, the freshwater from Irrawadi or Ganges-Brahmaputra also could affect the salinity in the region between 15 and 17°N. In order to understand the effect of circulation in redistributing the freshwater from the above-mentioned rivers, we analyzed monthly mean basin-wide geostrophic circulation during January derived from satellite-derived sea-level anomalies (Fig.13). It is clearly seen that the circulation south of 17°N along the east coast of India was southward, while that north of 17°N was northward. However, along the Myanmar coast the flow was southward. Hence there is less chance of freshwater input from Ganges-Brahmaputra or Irrawaddy to directly influence the salinity between the regions 15-17°N during winter. On the other hand, we notice an eastward advection of waters from the coastal region south of 17°N towards the central Bay into the study domain. This eastward advection, in addition to transporting winter-rain-driven freshwater discharge into the central Bay,

would also entrain the fresher shelf waters formed during the previous monsoon (summer) either locally or advected from the northern Bay of Bengal, into the study domain. Thus, the observed freshening in the regions 15-17°N during winter must be associated with the advection of freshwater from the rivers Godavari, Krishna and Pennar as well as the intrusion of fresher shelf waters formed during summer monsoon. The stratification associated with these low-salinity waters must be so strong that even a 4°C cooling in SST from summer to winter was unable to destroy the stratification and initiate convective mixing as happens in the case of the northern Arabian Sea (Prasanna Kumar and Prasad, 1996). In order to determine the degree of stratification, we calculated the static stability parameter (Pond and Pickard, 1983), which showed large stability values in the north in the upper 40 m for winter as well as summer (Fig.14, dashed line). This is due to the fact that density in the Bay of Bengal, especially in the northern Bay, is controlled by salinity rather than temperature. In fact the surface density distribution (not presented) is very similar to the surface salinity distribution with an annual variability of 3 kg/m<sup>3</sup> in the north and 1.5 kg/m<sup>3</sup> in the south. Thus, in the north the observed shallow time-invariant mixed layer results from the perennial presence of low-salinity water, which makes the upper ocean highly stratified throughout the year.

In the south the semi-annual variability of the mixed layer could be explained in terms of prevailing atmospheric forcing. During spring intermonsoon (March-May) the warmest SST associated with increased incoming solar radiation (~280 w/m<sup>2</sup>) and low salinity waters (32.5-33) results in a strong stratification. This low-salinity water is reminiscent of the freshwater input during summer due to the oceanic precipitation as well as river influx, which gets advected southward with time. Comparatively



lighter winds (4-6 m/s) occurring during this time of the year were unable to break the stratification by wind-driven turbulent mixing. Observed very shallow MLD ( $\sim 10\text{-}20$  m) is the manifestation of this process. As the season changed from spring intermonsoon to summer monsoon, the SST was cooled by about  $1.5^{\circ}\text{C}$  and wind peaked to its climatological maximum value (9 m/s). In addition to this, basin-wide geostrophic circulation and surface-salinity distribution for August (Fig.13) showed the intrusion of high-salinity waters of Arabian Sea origin, which aids in increasing the upper-layer density there by reducing the stratification. The static stability parameter showed extremely low values in the south in the upper 40 m (Fig.14b, solid line), and the increased wind speed during summer was capable of triggering a greater mixing. Thus, the deep MLD in the south resulted from the combined effect of wind-driven mixing and intrusion of high-salinity water from the Arabian Sea. In addition, the low net heat flux during this period in the south will also play a role in the vertical mixing. With the commencement of fall intermonsoon and secondary heating, the SST warmed nominally ( $\sim 0.5^{\circ}\text{C}$ ) and MLD decreased once again.

The deep mixed layers in the south during winter were puzzling, because the winter cooling was limited to north of  $15^{\circ}\text{N}$  as was evident from the SST. In the south SST was not cold enough to warrant winter convection, which would otherwise support a deep mixed layer. The static-stability parameter showed very low values (Fig.14a, solid line) and the surface salinity was around 34 in January when the deepest MLD (50 m) occurred. Also note that the wind speed at this time of the year was moderate (6 m/s). This suggests that the deep MLD in the south during winter, when the upper water column was comparatively less stable, must be driven by wind-mixing. Similarly, the occurrence of a deep MLD ( $\sim 30$  m) between  $15^{\circ}$  and

17°N during March to May was again a puzzle because the SST was high (~29°C) and surface salinity was low (~32.5), which under normal circumstances would support a shallow MLD as the static-stability parameter showed highly stable upper layers (Fig.14a) and winds were moderate (~6 m/s). This calls for an alternate mechanism. We explored the role of remote forcing via Rossby waves as a possible mechanism and used the monthly mean climatology of merged sea-level anomalies. The sloping contours in the time-longitude plots of SSH anomalies along 16°N indicated the signatures of westward-propagating Rossby wave (Fig.15a). During March to June we notice a positive sea-level anomaly in the study domain while for the rest of year the anomalies were mostly negative. We also used monthly-mean temperature and salinity data (Conkright et al., 2002) to determine the mixed layer depth. Monthly-mean climatology along 16°N showed negative MLD anomaly (Fig.15b) coinciding with the positive sea-level anomaly (Fig.15a) in the study domain during April to June. Note that the negative mixed-layer anomalies indicate a deep mixed layer, while the positive sea-level anomalies are linked to a thick surface layer. From the co-variation of mixed-layer depth and the sea-surface height during March to May, we conclude that it is the propagation of Rossby waves rather than the local atmospheric forcing that caused the deep MLD between 15° and 17°N. McCreary et al. (1996), with models, and Eigenheer and Quadfasel (2000), with the SSH anomalies derived from TOPEX/Poseidon, showed that remote forcing via Rossby-wave propagation plays the most important role for the sea level variability of the EICC. In addition to this, existence of warm-core eddies also may contribute to the deepening of the mixed layer.

The chlorophyll distribution available during spring intermonsoon and summer was strongly linked to the upper-ocean stratification and variability

in the mixed-layer depth. During spring intermonsoon the chlorophyll distribution showed a deep chlorophyll maximum (DCM) characteristic of the oligotrophic upper ocean. During this time of the year, when the incoming solar radiation was at its peak and winds were generally low, the mixed layer was very shallow and the upper layer was highly stratified. This inhibited any vertical mixing, and hence there was no input of nitrate from the subsurface to the upper ocean. At the same time, as there was no freshwater or sediment input from the peninsular rivers into the Bay during spring intermonsoon, the sunlight could penetrate deep, where there are enough nutrients to support biological production, resulting in the observed DCM. During summer the chlorophyll distribution did not show a DCM; instead a high concentration was observed in the upper 20 m in the north, with highest value at 20°N near the surface. As the freshwater discharge from peninsular rivers is at its peak during summer, it could be a potential nutrient source, especially in the north, for the enhanced biological productivity of the upper layers. Another mechanism that could enhance the biological productivity is the cold-core eddy. From recent measurements along the central Bay of Bengal, Prasanna Kumar et al. (2004) identified cold-core eddies and suggested upward eddy-pumping as one of the major mechanisms of nutrient supply to the euphotic zone. It may be recalled that the MLD was ~10 m in the north during summer with very strong stratification. The up/down sloping of nitrate isopleth centered at 18°N resulted in the injection of about 1  $\mu$ M nitrate to the surface waters. However, we do not see enhancement in the chlorophyll level in the vicinity of 14°N in spite of the up/down sloping of nitrate isopleths. The reason for very low chlorophyll concentrations noticed in the south, in spite of a

considerable quantity of nitrate in the upper 30 m, may be the coarse resolution in the chlorophyll data south of 17°N.

### **Acknowledgements**

We thank G.V. Reddy and J.S. Sarupriya for extracting hydrography data and chlorophyll data, respectively. Jayu Narvekar acknowledges the financial support from CSIR. This forms a part of the BOBDAT program supported by Space Application Centre, ISRO. This is NIO contribution number 4079.

## References

- Bathen, K.H., 1972. On the seasonal changes in the depth of mixed layer in the north Pacific Ocean. *Journal of Geophysical Research* 77, 7138-7150.
- Boyer, T.P., Levitus, S., Antonov, J.I., Conkright, M.E., O'Brien, T., Stephens, C., Trotsenko, B., 1998. World Ocean Atlas 1998: Vol. 6: Salinity of the Indian Ocean. NOAA Atlas NESDIS 32, U.S. Government Printing Office, Washington, D.C.
- Conkright, M., Levitus, S., O'Brien, T., Antonov, J., Stephens, C., 1998. World Ocean Atlas 1998 CD-ROM Data Set Documentation, Technical Report 15, National Oceanographic Data Center, Silver Spring, Md.
- Conkright, M., Locarnini, R.A., Garcia, H.E., O'Brien, T.D., Boyer, T.P., Stephens, C., Antonov, J.I., 2002. World Ocean Atlas 2001: Objective analyses, data statistics, and figures CD-ROM Documentation, Technical Report 17, National Oceanographic Data Center, Silver Spring, Md.
- Da Silva, A., Young, A.C., Levitus, S., 1994. Atlas of surface Marine data 1994, Vol.1: Algorithms and Procedures. NOAA Atlas NESDIS 6, US Department of Commerce, Washington, DC.
- Eigenheer, A., Quadfasel, D., 2000. Seasonal variability of the Bay of Bengal circulation inferred from TOPEX/Poseidon altimetry. *Journal of Geophysical Research* 105, 3243-3252.
- Gopalakrishna, V.V., Sadhram, Y., Ramesh Babu, V., 1988. Variability of mixed layer depth in the northern Indian Ocean during 1977 and 1979 summer monsoon seasons, *Indian Journal of Marine Sciences* 17, 258-264.
- Josey, S. A., Kent, E. C. and Taylor, P. K., 1998. The Southampton Oceanography Centre (SOC) Ocean - Atmosphere Heat, Momentum and Freshwater Flux Atlas, *Southampton Oceanography Centre Report No. 6*, 30 pp. plus figs.
- Levitus, S., 1982. Climatological Atlas of the World Ocean, NOAA Professional paper 13, National Oceanic and Atmospheric Administration, Rockville Md, 173 pp.
- Levitus, S., Gelfeld, R., Boyer, T., Johnson, D., 1994. Results of the NODC Oceanographic Data Archaeology and Rescue Projects, Key to Oceanographic Records Documentation No. 19, NODC, Washington, D.C., 73pp.
- Lukas, R., Lindstrom, E., 1991. The mixed layer of western equatorial Pacific Ocean. *Journal of Geophysical Research* 96, 3343-3357.
- McCreary, J.P., Kundu, P.K., Molinari, R.L., 1993. A numerical

- investigation of dynamics, thermodynamics and mixed-layer processes in the Indian Ocean. *Progress in Oceanography* 31, 181-244.
- McCreary, J.P., Han, W., Shankar, D., Shetye, S.R., 1996. Dynamics of the East India Coastal Current, 2, Numerical solutions. *Journal of Geophysical Research* 101, 13993-14010.
- Molinari, R.L., Swallow, J., Festa, J.F., 1986. Evolution of the near-surface thermal structure in the western Indian Ocean during FGGE 1979. *Journal of Marine Research* 44, 739-762.
- Monterey, G., Levitus, S., 1997. Seasonal variability of mixed layer depth for the world ocean, NOAA atlas NESDIS 14, U.S. Gov. Printing Office, Washington, D.C., 87 figures & 96pp.
- Prasad, T.G., 1997. Annual and seasonal mean buoyancy fluxes for the tropical Indian Ocean. *Current Science* 73, 667-674.
- Prasad, T.G., 2004. A comparison of mixed layer dynamics between the Arabian Sea and the Bay of Bengal: one dimensional model results. *Journal of Geophysical Research*, 109, doi:10.1029/2003JC002000.
- Perigaud, C., Delecluse, P., 1992. Annual sea level variations in the southern tropical Indian Ocean from geosat and shallow-water simulations. *Journal of Geophysical Research* 97, 20169-20178.
- Pond, S., Pickard, G.L., 1983. *Introductory dynamical oceanography*, Pergamon Press, New York, 241pp.
- Potemra, J.T., Luther, M.E., O'Brien, J.J., 1991. The seasonal circulation of the upper ocean in the Bay of Bengal. *Journal of Geophysical Research* 96, 12667-12683.
- Prasanna Kumar, S., Unnikrishnan, A.S., 1995. Seasonal cycle of temperature and associated wave phenomena in the upper layers of the Bay of Bengal. *Journal of Geophysical Research*, 100, 13585-13593.
- Prasanna Kumar, S., Prasad, T.G., 1996. Winter cooling in the northern Arabian Sea. *Current Science* 71, 834-841.
- Prasanna Kumar, S., Nuncio, M., Jayu Narvekar, Ajoy Kumar, Sardesai, S., Desouza, S.N., Mangesh Gauns, Ramaiah, N. and Madhupratap, M., 2004. Are Eddies nature's trigger to enhance biological productivity in the Bay of Bengal?, *Geophysical Research Letters*. 31, L07309, doi:10.1029/2003GL019274.
- Rao, R.R., 1986. Cooling and deepening of the mixed layer in the central Arabian Sea during Monsoon-77: Observations and simulations. *Deep-Sea Research* 33, 1413-1424.
- Rao, R.R., Molinari, R.L., Festa, J.F., 1989. Evolution of the climatological near-surface thermal structure of the tropical Indian Ocean: 1 Description of mean monthly mixed-layer depth and sea-surface temperature, surface-

- current and surface meteorological fields. *Journal of Geophysical Research* 94, 1081-10815.
- Sanilkumar, K.V., Kuruvilla, T.V., Jogendranath, D., Rao, R.R., 1997. Observations of the western boundary current of the Bay of Bengal from a hydrographic survey during March 1993. *Deep-Sea Research I* 44, 135-145.
- Schneider, N., Muller, P., 1990. The meridional and seasonal structures of the mixed layer depth and its diurnal amplitude observed during the Hawaii-to-Tahiti Shuttle Experiment *Journal of Physical Oceanography* 20, 1395-1404.
- Shenoi, S.S.C., Shankar, D., Shetye, S.R., 2002. Difference in heat budgets of the nearsurface Arabian Sea and Bay of Bengal: Implications for the summer monsoon, *Journal of Geophysical Research*, 107, doi:10.1029/2000JC000679.
- Schott, F.A., McCreary, J.P., 2001. The monsoon circulation of the Indian Ocean. *Progress in Oceanography* 51, 1-123.
- Shankar, D., McCreary, J.P., Han, w., Shetye, S.R., 1996. Dynamics of the East India Coastal Current, 1, Analytic solutions forced by interior Ekman pumping and local alongshore winds. *Journal of Geophysical Research* 101, 13975-13991.
- Shankar, D., Vinayachandran, P.V., Unnikrishnana, A.S., 2002. The monsoon currents in the north Indian Ocean. *Progress in Oceanography* 52, 63-120.
- Shetye S.R., Gouveia, A.D., Shenoi, S.S.C., Sundar, D., Michael, G.S., Almeida, A.A., Santanam, K., 1991. The coastal currents off western India during north east monsoon. *Deep-Sea Research Part A* 38, 1517-1529.
- Shetye, S.R., Gouveia, A.D., Shenoi, S.S.C., Sundar, D., Michael, G.S., Nampothiri, G., 1993. The western boundary current of the seasonal subtropical gyre in the Bay of Bengal, *Journal of Geophysical Research* 98, 945-954.
- Shetye, S.R., Gouveia, A.D., Shenoi, S.S.C., Shankar, D., Vinayachandran, P.N., Sundar, D., Michael, G.S., Nampothiri, G., 1996. Hydrography and circulation and circulation in the western Bay of Bengal during the northeast monsoon, *Journal of Geophysical Research* 101, 14011-14025.
- Subramanian, V., 1993. Sediment load of Indian Rivers, *Current Science* 64, 928-930.
- UNESCO, 1981. Technical papers in marine science. United Nations Educational, Scientific and Cultural Organization, Paris, 192pp.
- Varkey, M.J., Murty, V.S.N., Suryanarayana, A., 1996. Physical oceanography of the Bay of Bengal and Andaman Sea. *Oceanography and*

- Marine Biology: an Annual Review 34, 1-70.
- Vinayachandran, P.N., Shetye, S.R., Sengupta, D., Gadgil, S., 1996. Forcing mechanisms of the Bay of Bengal circulation. *Current Science* 71, 753-763.
- Yu, L., O'Brien, J.J., Yang, J., 1991. On the remote forcing of the circulation in the Bay of Bengal. *Journal of Geophysical Research* 96, 20449-20454.
- Wyrski, K., 1964. The thermal structure of the eastern Pacific Ocean, *Dtsch. Hydrogr. Ze.*, Supplement A8, 6-84.



Table 1. Number of temperature and salinity profiles in each of the 2° latitude (4-20°N) x 4° longitude (87-91°) bins for each month. The dash (-) line indicates no data. Total number of profiles: 492.

Month	2° latitude x 4° longitude bin							
	4-6	6-8	8-10	10-12	12-14	14-16	16-18	18-20
January	3	-	2	-	7	7	1	-
February	5	-	-	1	7	-	-	4
March	-	-	-	-	2	-	5	23
April	-	2	2	5	10	13	14	14
May	-	-	-	-	5	-	-	-
June	-	2	5	7	2	5	-	2
July	-	6	6	8	4	11	27	24
August	5	-	7	3	2	2	12	29
September	7	4	10	10	10	9	5	9
October	13	7	12	5	11	8	2	1
November	-	-	2	5	9	10	3	-
December	1	-	4	5	3	6	4	16

Table 2. Number of nitrate and chlorophyll (within parentheses) profiles in each of the 2° latitude (4-20°N) x 4° longitude (87-91°) bins for each month. The dash (-) line indicates no data. Total number of profiles nitrate: 89 and chlorophyll: 83.

Season	2° latitude x 4° longitude bin							
	4-6	6-8	8-10	10-12	12-14	14-16	16-18	18-20
<b>Spring Intermonsoon</b> (March-May)	- (-)	- (2)	1 (2)	1 (1)	4 (3)	2 (6)	3 (13)	2 (14)
<b>Summer monsoon</b> (June- September)	1 (2)	3 (-)	2 (-)	4 (-)	5 (3)	8 (3)	13 (3)	17 (13)
<b>Fall Intermonsoon</b> (October)	2 (-)	1 (-)	- (-)	- (-)	3 (-)	- (-)	- (-)	- (-)
<b>Winter monsoon</b> (November-February)	3 (-)	12 (7)	- (-)	- (-)	- (-)	- (1)	- (2)	2 (8)

## Legend to figures

Fig. 1. Location map showing the annual mean salinity distribution (Levitus et al., 1994) in the Bay of Bengal. The rectangle (4-20°N, 87-91°E) indicates the region within which the data is analysed. Rivers Ganges, Brahmaputra, Mahanadi, Godavari, Krishna and Irawady are also shown. Depth contours are in meters. The region filled with dots along the east coast of India indicates the meteorological subdivision coastal Andhra Pradesh where rainfall data is analysed.

Fig.2 Vertical profiles of temperature (solid line), salinity (broken line) and density (sigma-t; dash-dot line) for August (a,b) and February (c,d) for a 2-degree grid centered at 11°N (a,c) and 19°N (b,d) along 89°E.

Fig.3 Time-latitude plot of mixed layer depth (MLD, m) along 89°E. The stippled region indicates MLD deeper than 30 m. The dots indicate data locations.

Fig.4 Time-latitude plot of sea-surface temperature (SST, °C) along 89°E. The stippled region indicates SST colder than 27°C during winter and warmer than 28.5°C during fall intermonsoon. The dots indicate data locations.

Fig.5 Time-latitude plot of sea-surface salinity (SSS) along 89°E. The stippled region indicates salinity lower than 32.0. The dots indicate data locations.

Fig.6 Time-latitude plot of short-wave radiation ( $w/m^2$ ) along 89°E. Stippled regions indicate values greater than 280  $w/m^2$  and 220  $w/m^2$  during spring and fall intermonsoons, respectively. The dots indicate data locations.

Fig.7 Time-latitude plot of net heat flux ( $w/m^2$ ) along 89°E. Stippled regions indicate heat loss from the ocean.

Fig.8 Time-latitude plot of wind speed (m/s). Stippled region indicates values greater than 9 m/s and 6 m/s during summer and winter monsoon, respectively. The dots indicate data locations.

Fig.9 Time-latitude plot of E-P (mm/month) along 89°E. Stippled region shows precipitation exceeds evaporation by 120 mm/month. The dots indicate the data locations.

Fig.10 Vertical distribution of nitrate ( $\mu\text{M}$ ) along 89°E during (a) spring intermonsoon and (b) summer. Note that summer data is from 12°N only. The dots indicate the data locations.

Fig.11 Chlorophyll concentrations ( $\text{mg}/\text{m}^3$ ) derived from (a,c) SeaWiFS and (b,d) *in situ* data along 89°E during spring intermonsoon (a,b) and summer monsoon (c,d). See text for details. Note that during summer the vertical distribution is from 12°N. The dots indicate the data locations.

Fig.12 (a) Climatological winter rainfall (mm) during November to February at Coastal Andhra Pradesh (1871-2000), east coast of India and Yangon (1961-1990), west coast of Myanmar and (b) river discharge ( $\text{m}^3$ ) during December to March of Godavari (1901-1979), Krishna (1901-1979) and Pennar (1965-1979). Numbers on the top of the histogram in (a) indicates contribution of winter rainfall to the annual rainfall.

Fig.13 Monthly mean climatology of surface salinity (Boyer et al. 1998) overlaid with geostrophic velocity (vector, m/s) derived from climatology of Topex/Poseidon ERS1/2 merged sea-level anomaly for January (top) and August (bottom).

Fig.14 Profiles of upper-ocean static-stability parameter ( $E, \text{m}^{-1}$ ) at 17°N (dashed line) and 13°N (solid line) in the Bay of Bengal during (a) January and (b) August.

Fig.15 Time-longitude plot of monthly mean climatology (October 1992 to January 2004) of (a) merged sea-level anomaly (cm) (Topex/Poseidon ERS1/2 satellites obtained from AVISO, see text for details) and (b) mixed layer depth anomaly (m) along 16°N. Starting month is June. Stippled region indicates positive sea-level anomaly and negative mixed layer depth anomaly respectively.

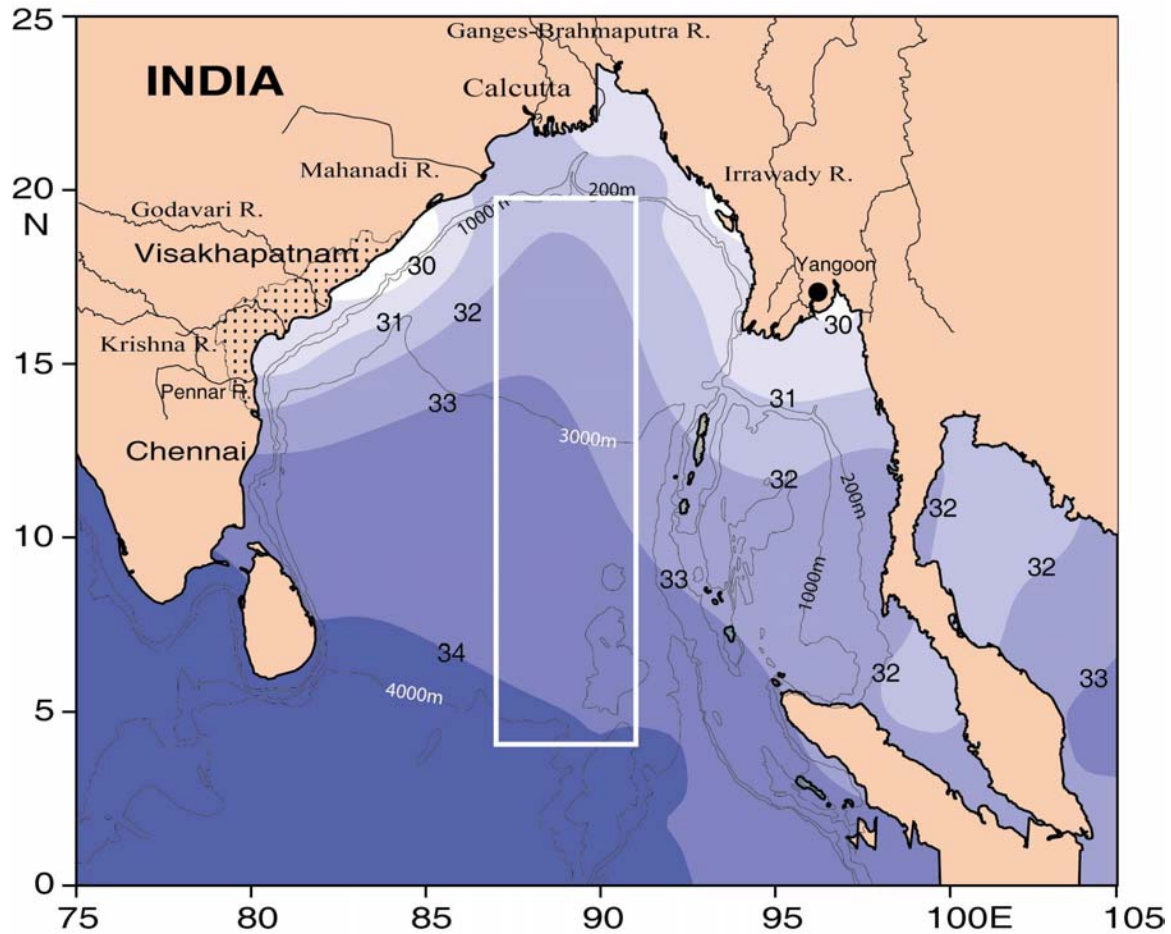


Fig.1. Location map showing the annual mean salinity (psu) distribution (Levitus et al., 1994) in the Bay of Bengal. The rectangle (4-20°N, 87-91°E) indicates the region within which the data is analysed. Rivers Ganges-Brahmaputra, Mahanadi, Godavari, Krishna, Pennar and Irrawady are also shown. Depth contours are in meters. The region filled with dots along the east coast of India indicates the meteorological subdivision coastal Andhra Pradesh where rainfall data is analysed.

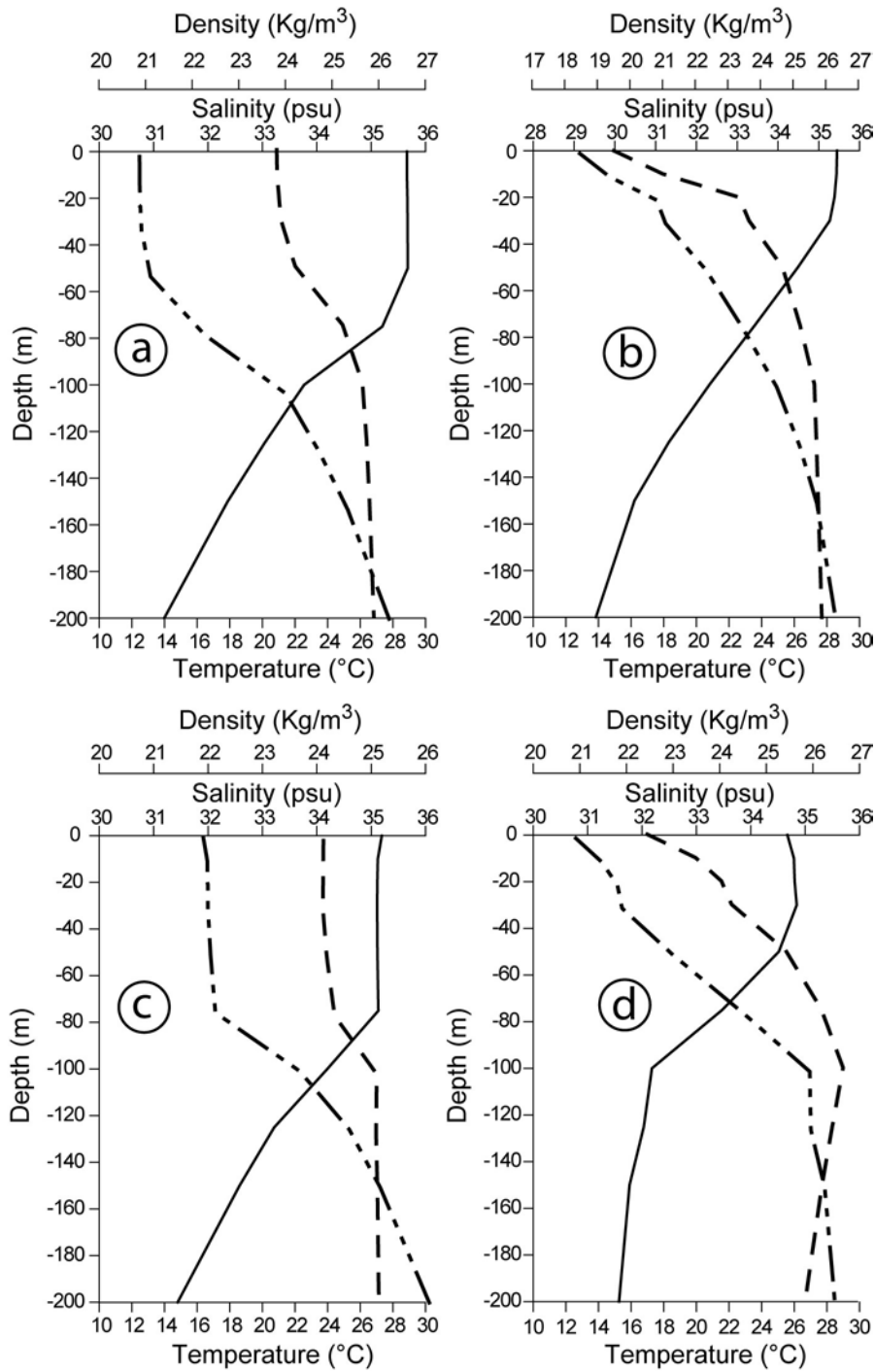


Fig.2 Vertical profiles of temperature (solid line), salinity (broken line) and density (sigma-t; dash-dot line) for August (a,b) and February (c,d) for a 2-degree grid centered at 11°N (a,c) and 19°N (b,d) respectively along 89°E.

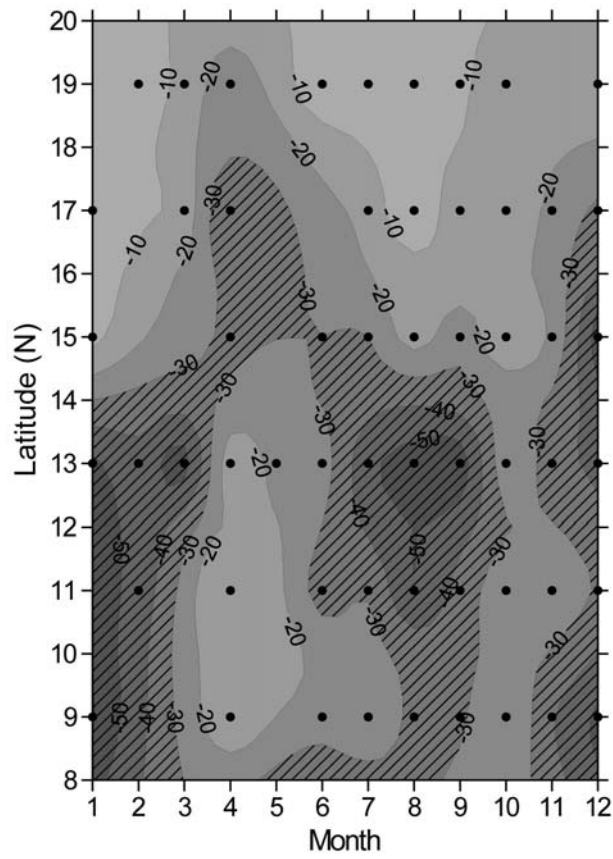


Fig.3 Time-Latitude plot of mixed layer depth (MLD,m) along 89°E. The stippled region indicates MLD deeper than 30m. Black dots indicate data points.

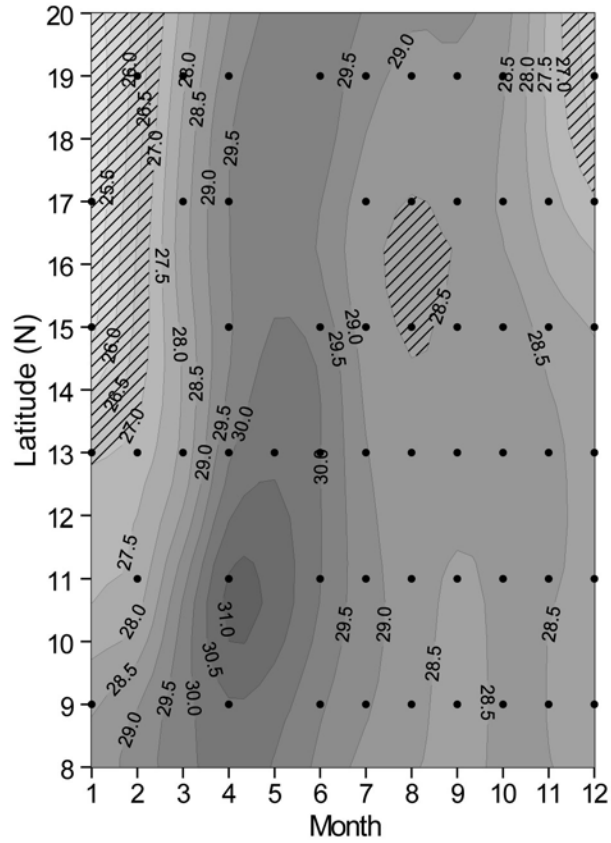


Fig.4 Time-Latitude plot of sea surface temperature (SST, °C) along 89°E. The stippled region indicates SST colder than 27°C during winter and warmer than 28.5°C during fall Intermonsoon. (August-September). Black dots indicate data points.

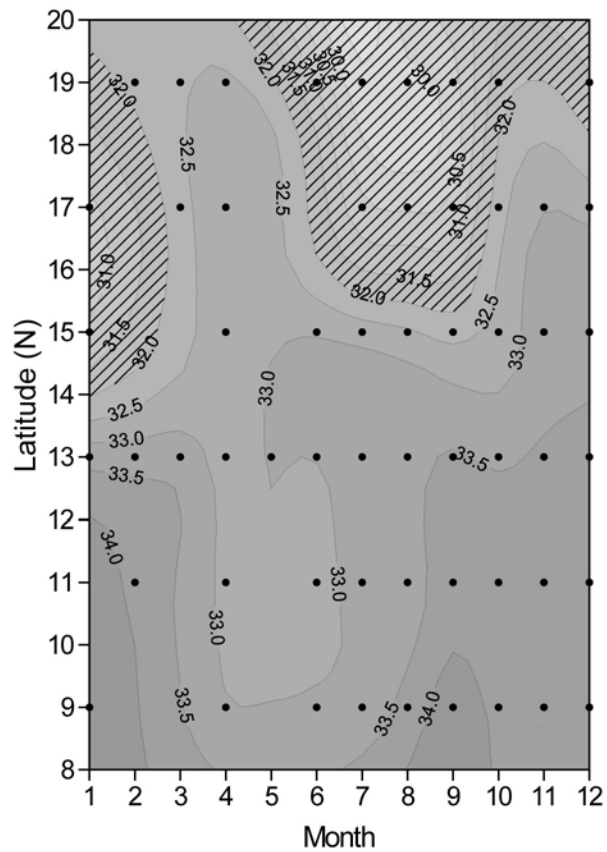


Fig.5 Time-Latitude plot of sea surface salinity (SSS, psu) along 89°E. The stippled region indicates salinity lower than 32psu. Black dots indicate data points.



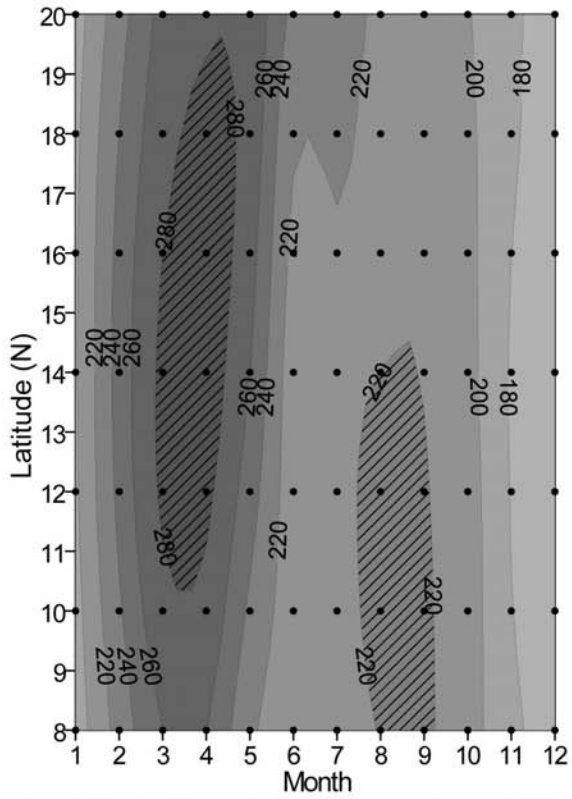


Fig.6 Time-Latitude plot of short wave radiation ( $W/m^2$ ) along  $89^\circ E$ . Stippled regions indicate values greater than  $280 W/m^2$  and  $220 W/m^2$  during spring and fall Intermonsoons respectively. Black dots indicate data points.

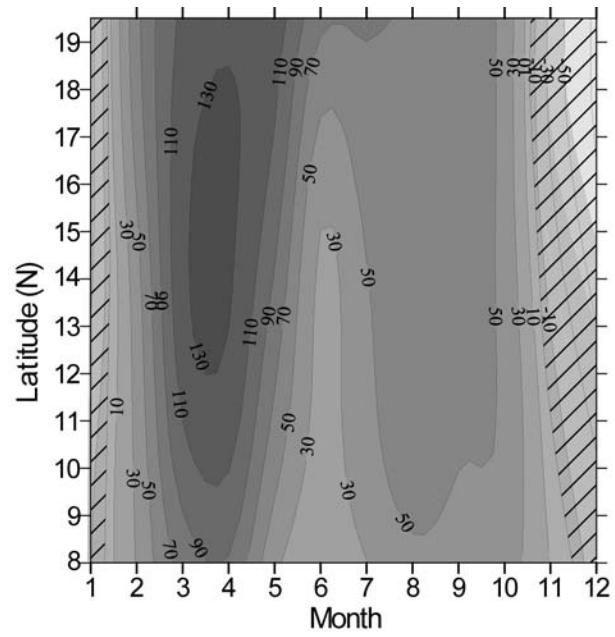


Fig.7 Time-Latitude plot of net heat flux ( $w/m^2$ ) along  $89^\circ E$ . Stippled regions indicate heat loss from the ocean.

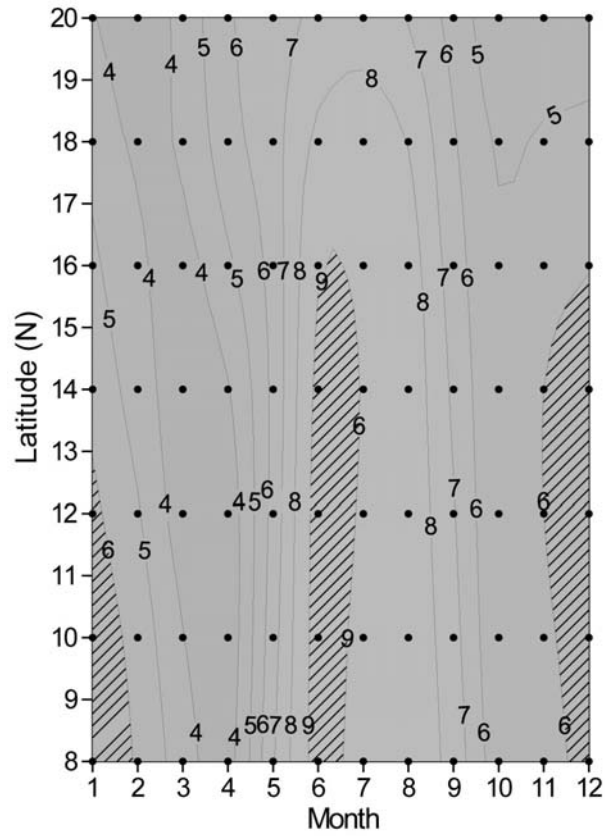


Fig.8 Time-Latitude plot of wind speed (m/s). Stippled region indicates values greater than 9m/s and 6m/s during summer and winter monsoon respectively. Black dots indicate data points.

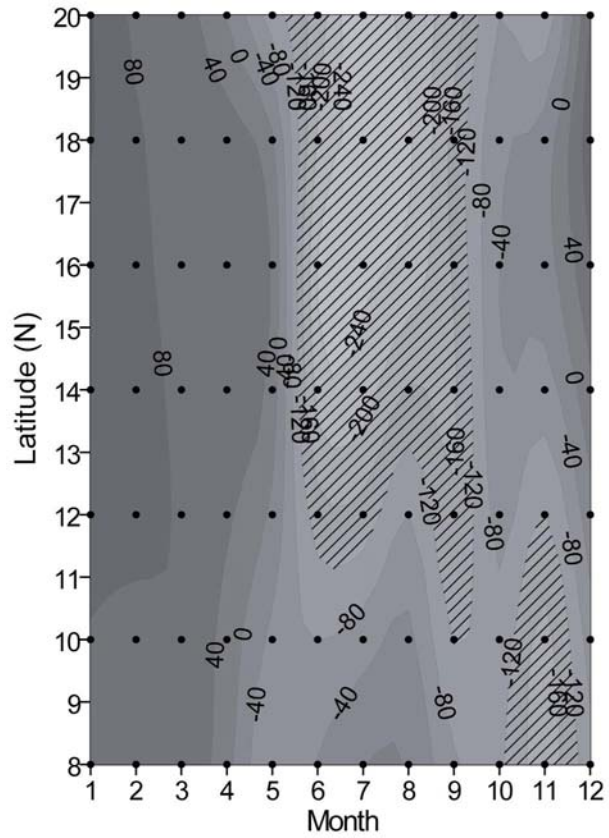


Fig.9 Time-Latitude plot of E-P (mm/month) along 89°E. The stippled region shows precipitation exceeds evaporation by 120mm/month. Black dots indicate data points.

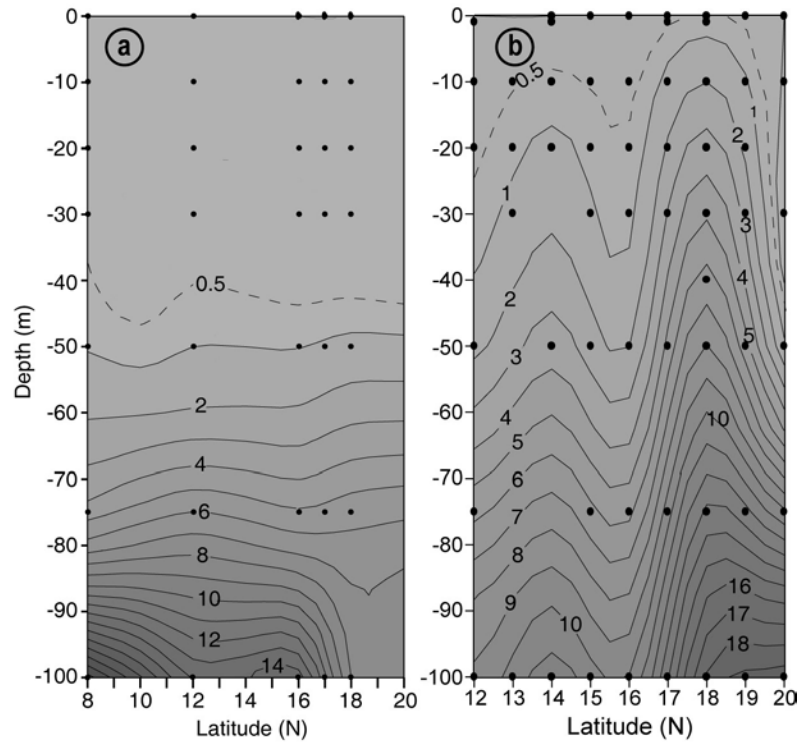


Fig.10 Vertical distribution of nitrate ( $\mu\text{mole}$ ) along  $89^\circ\text{E}$  during (a) spring Intermonsoon and (b) summer. Note that summer data is from  $12^\circ\text{N}$  only. Black dots indicate data points.

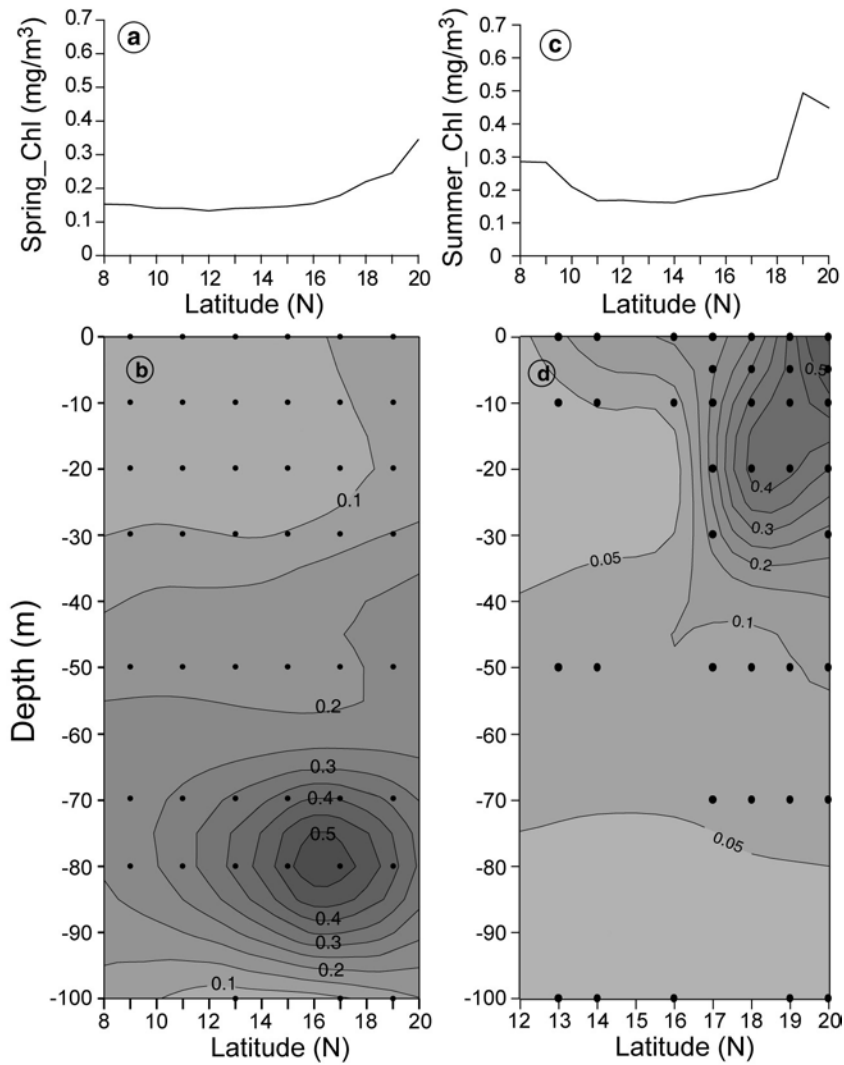


Fig.11 Chlorophyll concentrations ( $\text{mg}/\text{m}^3$ ) derived from (a,c) SeaWiFS and (b,d) *in situ* data along  $89^\circ\text{E}$  during spring Intermonsoon (a,b) and summer monsoon (c,d). See text for details. Note that during summer the vertical distribution is from  $12^\circ\text{N}$ . Black dots indicate data points.

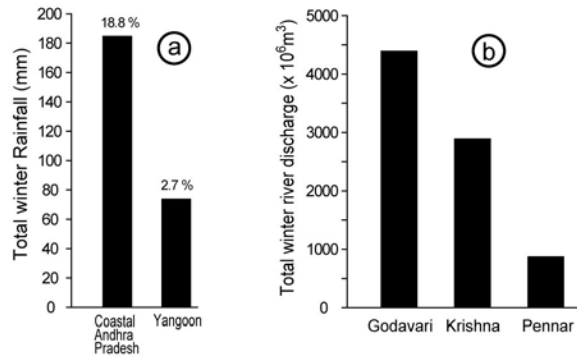


Fig.12 Climatological winter (a) rainfall (mm) during November to February at Coastal Andhra Pradesh (1871-2000), east coast of India and Yangon (1961-1990), west coast of Myanmar and (b) river discharge ( $\text{m}^3$ ) during December to March of Godavari (1901-1979), Krishna (1901-1979) and Pennar (1965-1979) . Numbers on the top of the histogram in (a) indicates contribution of winter rainfall to the annual rainfall.

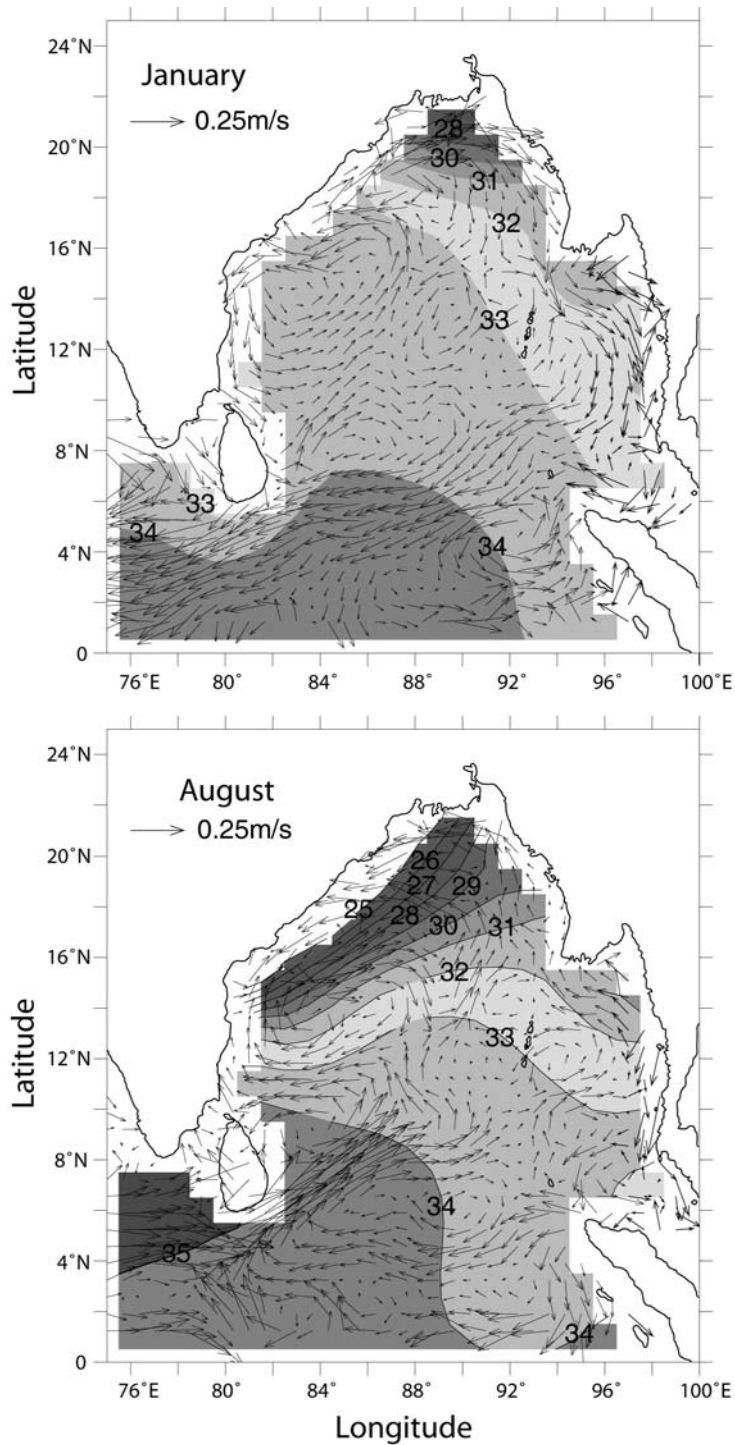


Fig.13 Monthly mean climatology of surface salinity (psu) (Boyer *et al.* 1998) overlaid with geostrophic velocity (vector, m/s) derived from climatology of Topex/Poseidon ERS1/2 merged sea-level anomaly for January (top) and August (bottom).



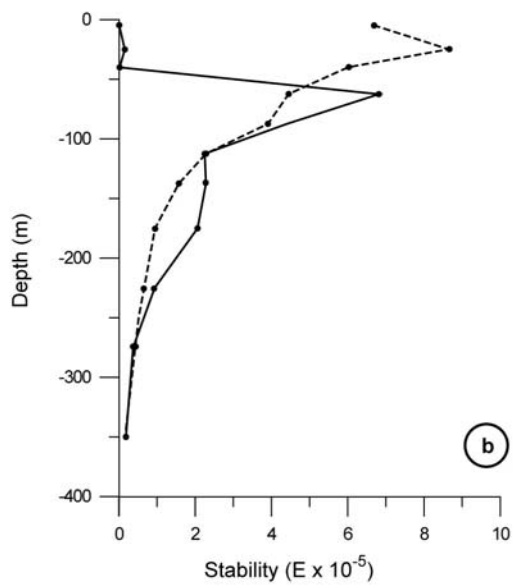
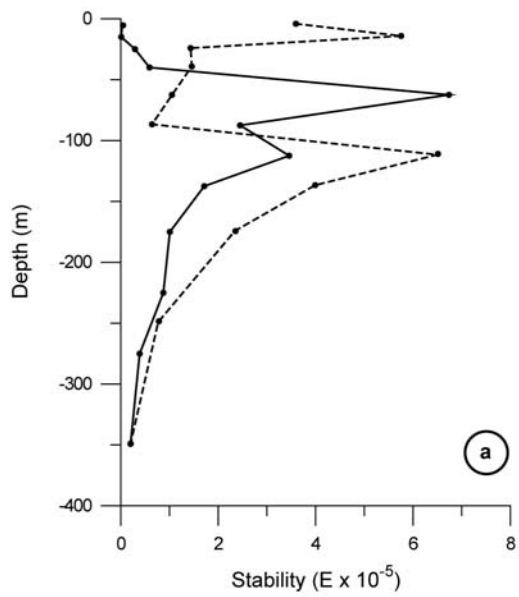


Fig.14 Profiles of upper ocean static stability parameter ( $E, m^{-1}$ ) at  $17^{\circ}N$  (dashed line) and  $13^{\circ}N$  (solid line) in the Bay of Bengal during (a) January and (b) August.

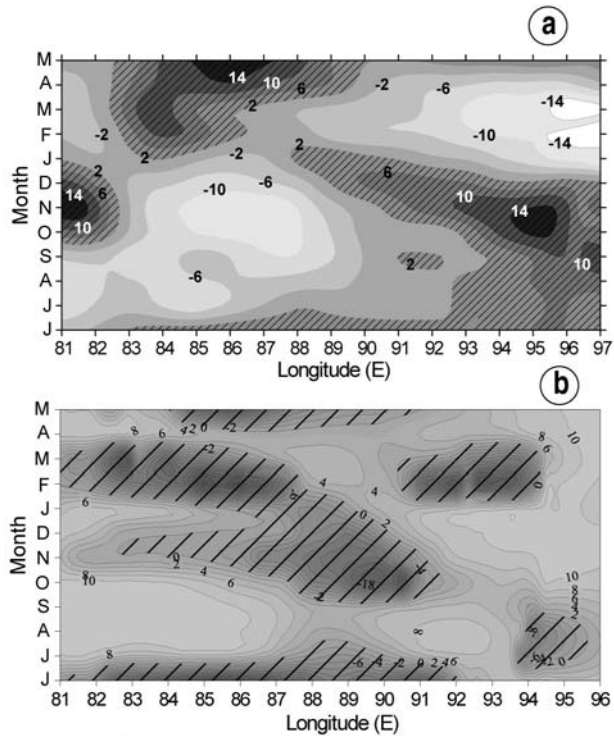


Fig.15 Time-Longitude plot of monthly mean climatology (October 1992 to January 2004) of merged sea-level anomaly (cm) (Topex/Poseidon ERS 1/2 satellites obtained from AVISO, see text for details) and (b) mixed layer depth anomaly (m) along 16°N. Starting month is June. Stippled region indicates +ve sea-level anomaly and -ve mixed layer depth anomaly respectively.